

# OTOLARYNGOLOGY/HEAD AND NECK SURGERY COMBAT CASUALTY CARE IN OPERATION IRAQI FREEDOM AND OPERATION ENDURING FREEDOM

## Section VI: Delayed Head and Neck Surgery/Treatment at the Role 4 Facility



Sandstorm, Balad Air Base, Iraq (2004).

Photograph: Courtesy of Colonel Joseph A. Brennan.



# Chapter 33

## PREOPERATIVE PLANNING FOR DELAYED HEAD AND NECK SURGERY

JOSE E. BARRERA, MD, FACS,\* AND CECELIA E. SCHMALBACH, MD, FACS†

---

INTRODUCTION

VIRTUAL SURGICAL PLANNING

ORBITAL RECONSTRUCTION

ZYGOMATICOMAXILLARY COMPLEX FRACTURES

MAXILLARY-MANDIBULAR RECONSTRUCTION

SUMMARY

CASE PRESENTATIONS

Case Study 33-1: Medical Modeling for Mandibular Reconstruction

Case Study 33-2: Medical Modeling in Combined Mandibular Reconstruction and  
Maxillary Reconstruction

\*Lieutenant Colonel, Medical Corps, US Air Force; Chairman, Department of Otolaryngology, San Antonio Military Medical Center, 3551 Roger Brooke Drive, Joint Base San Antonio, Fort Sam Houston, Texas 78234-5004; Associate Professor of Surgery, Uniformed Services University of the Health Sciences

†Lieutenant Colonel, Medical Corps, US Air Force; Associate Professor of Surgery, Otolaryngology Residency Program Director, Head & Neck Microvascular Surgery, Division of Otolaryngology, The University of Alabama at Birmingham, 1720 Second Avenue South, Birmingham, Alabama 35294-0012

## INTRODUCTION

Modern surgical planning now involves stereolithography and computer-assisted surgery to aid in reconstructing maxillofacial defects. Although the literature is devoid of experience stemming from Operation Iraqi Freedom and Operation Enduring Freedom, several articles describe the use of computed tomography (CT) to plan and guide surgical reconstruction. With advancements in software technology and 3-dimensional (3D) printing, bony reconstruction can methodically and predictably be achieved.

The development of digital imaging and communications in medicine (DICOM), with various proprietary software, includes programs created for surgical planning in craniomaxillofacial reconstruction. The treatment of complex maxillofacial trauma is difficult to plan, articulate, and execute, and using CT alone to plan does not take into account the 3D complexities required in surgical reconstruction. Using 3D formatting helps the surgeon understand the extent of anatomic distortion and bony comminution and displacement; however, it offers little information in terms of estimating injured blood vessels and

tissue avulsion. Performing standard head and neck examinations, with particular attention to zones of injury, and following Advanced Traumatic Life Support protocols are essential and should not be overlooked in anticipation of obtaining radiologic information. Surgical planning for facial trauma involves understanding occlusal norms and performing proper facial analysis to minimize postoperative deformity. Bony continuity is paramount in achieving these aims.

Complex facial injuries may involve loss of dentition and bone fractures that require prior surgical planning to achieve optimal results. Dental cast modeling is useful in preoperative planning; the casts are laser scanned and virtually integrated into imaging data. The use of occlusal splints based on computer-aided design and computer-aided modeling (CAD/CAM) has also improved surgical accuracy in reconstructing the mandible and midface.<sup>1</sup> This technique provides a similar benefit in cases of facial trauma when loss of teeth or tooth-bearing bony segments, and comminuted or severely displaced bone is present.

## VIRTUAL SURGICAL PLANNING

The use of 3D virtual surgical planning (VSP) and modeling for the treatment of complex orthognathic reconstruction allows surgeons to optimally reposition the craniofacial skeletal fragments, provides splints to assist in and confirm alignment, and provides templates for bone replacement or augmentation. If these virtual tools and techniques are combined with guidance technology, bone position can be examined closely throughout the operation. VSP is a computer-aided surgical simulation that is developed in four phases. The clinical data phase involves an ear, nose, and throat examination and airway assessment, including dental skeletal models using a reference for occlusion, and standard radiographs to document cephalometric norms. The second phase in virtual planning is integrating the 3D CT data with the dental model using proprietary virtual planning software and marrying the surgeon's expertise with that of a computer engineer.

The second phase of VSP involves meeting with an engineer to discuss the goals of the surgical team. Virtually, the comminuted segments can be reduced to achieve native bony alignment, and the appropriate dentoalveolar arch can be estimated. Splints can be fabricated when warranted to be used to obtain occlusal relationship. Facial height and width analysis can be performed to assist the trauma surgeon when disimpaction of fractured segments must be accounted for to obtain symmetry. From this analysis, templates

can be created and fabrication of custom plates, if desired, can also be done. In addition to the temporary intraoperative guides or splints that allow for optimal reduction, virtual surgery affords the opportunity for the design of precise permanent implants. These can be either autologous tissue (bone graft) or alloplastic implants (titanium mesh or titanium reconstruction plates) depending on the operative need.<sup>1</sup>

Third, the surgical phase involves the virtual plan for maxillofacial surgery using computer-aided fabrication of surgical splints and templates. An intermediate splint is fabricated and used to register maxillary and mandibular occlusion in advancement and pan-facial trauma cases, and a final splint is used for final occlusive reference. The splint is essential to articulate the occlusal reference when this relationship is absent in the natively injured pan-facial fracture patient. The final phase compares the surgical accuracy of VSP to the preoperative state by determining the extent of reduction achieved with bony fixation in the maxillofacial skeleton and how this impacts facial symmetry, the final occlusion achieved, and aesthetic outcomes of the surgery (Figure 33-1). Accuracy of impaction, advancement, and plate fixation can be assessed, and a comparison of the postsurgical result to the presurgical plan can be rendered. Postoperative CT scans can be used to evaluate the implementation of the treatment plan and analyze any deviations.

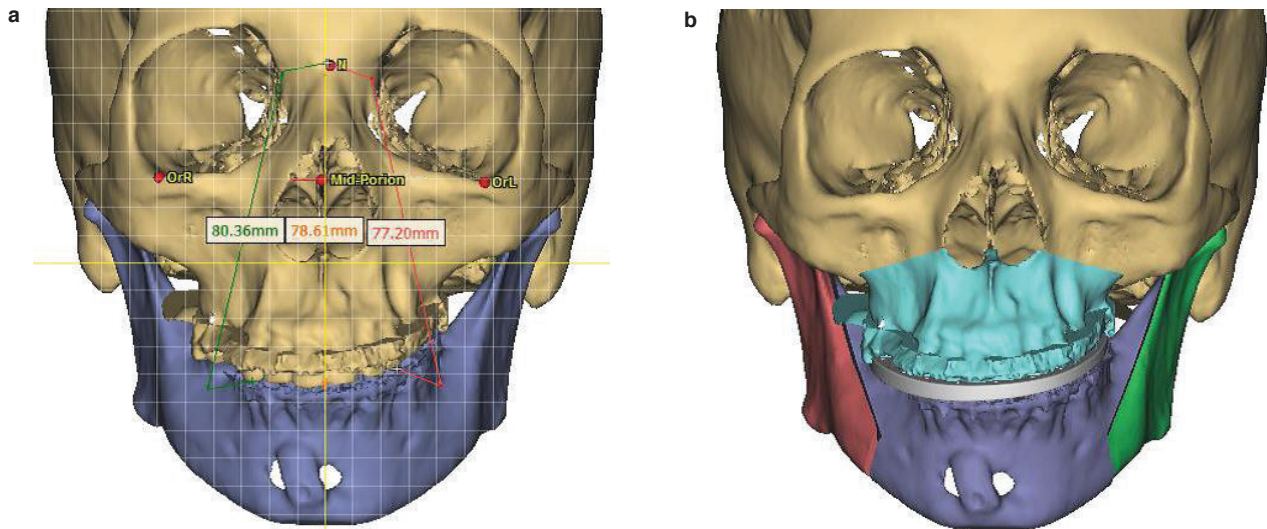


**Figure 33-1.** Virtual surgical plan for a patient who underwent bimaxillary advancement surgery. A 3-mm cant can be assessed preoperatively (a), and appropriate splint therapy associated with planned advancement and impaction can be used to ensure stabilization of maxillary-mandibular complex. Accuracy of impaction, advancement, and plate fixation can be assessed, and a postsurgical result emulating the presurgical plan can be rendered (b). OrL: orbitale left; OrR: orbitale right.

## ORBITAL RECONSTRUCTION

Orbital reconstruction of traumatic blow-out fractures has traditionally used CT to analyze the position of bony fragments, estimate volume loss, and clinically predict the impact on extraocular muscle function. In combination with a thorough ophthalmologic and head and neck examination, functional and aesthetic deficits are documented. However, common errors due to undercorrection or overcorrection of orbital bone alignment and volume have led to frequent reoperations and possible complications. The use of computer-assisted preoperative planning helps to obviate these problems by accurately predicting volume loss and determining the appropriate type and size of implant to be used. The importance of orbital volume measurement for orbital wall fractures is well recognized.<sup>2-4</sup> Orbital volume can be measured from axial scans by delineating the bony orbital walls.<sup>4-7</sup> However, it is difficult to calculate orbital volume in floor fractures from axial scans, whereas a coronal scan offers excellent diagnostic information for orbital floor fractures and may provide a more accurate measure.<sup>8</sup> Several recent reports estimate the bony orbital volume by using coronal-plane scans.<sup>9,10</sup>

Clinical applications of 3D CT technology are numerous. In a novel approach to estimating 3D orbital volume, Kwon et al evaluated the cephalometric determination of orbital volume using stereoscopic 3D CT scans.<sup>11</sup> Many prior studies of orbital volume were conducted using axial CT scans alone.<sup>3-6</sup> Although several groups have reported estimates of the bony orbital volume using coronal scans, Kwon's study was the first

to compare orbital volume from different planes. The criterion for the anterior limit of measurement can affect volume determination. Three novel cephalometric angles that can be obtained by 3D image analysis with stereoscopy were described, which may account for the inaccuracies seen on coronal scans.<sup>11</sup> Therefore, it is important to evaluate the orbital volume calculation from coronal scans (Figure 33-2A) as well from axial scans (Figure 33-2B).

Orbital blowout fractures are some of the most common injuries observed in the facial region, and one of the most important goals of reconstructing orbital wall fractures is restoration of normal orbital volume.<sup>5</sup> Therefore, accurate preoperative measurement of orbital volume is invaluable in predicting and, if it leads to operative intervention, preventing postinjury enophthalmos, a common complication.<sup>5</sup> Furthermore, orbital volume measurements can provide an accurate estimation of orbital implant volume, which is necessary for optimal reconstruction of enophthalmos. However, several problems can arise when CT scans are used to measure the orbital volume with standard computer-based programs. Difficulties in measuring the exact orbital volume include (a) the shape of bony orbital cavities, which are roughly the shape of a quadrilateral pyramid with its base directed forward and laterally, not located exactly horizontal or perpendicular to the axial or coronal plane<sup>7</sup>; (b) bony defects, which in some locations can cause errors in measurement (eg, orbital apex, inferior orbital fissure, superior orbital fissure, lacrimal sac, and orbital base,

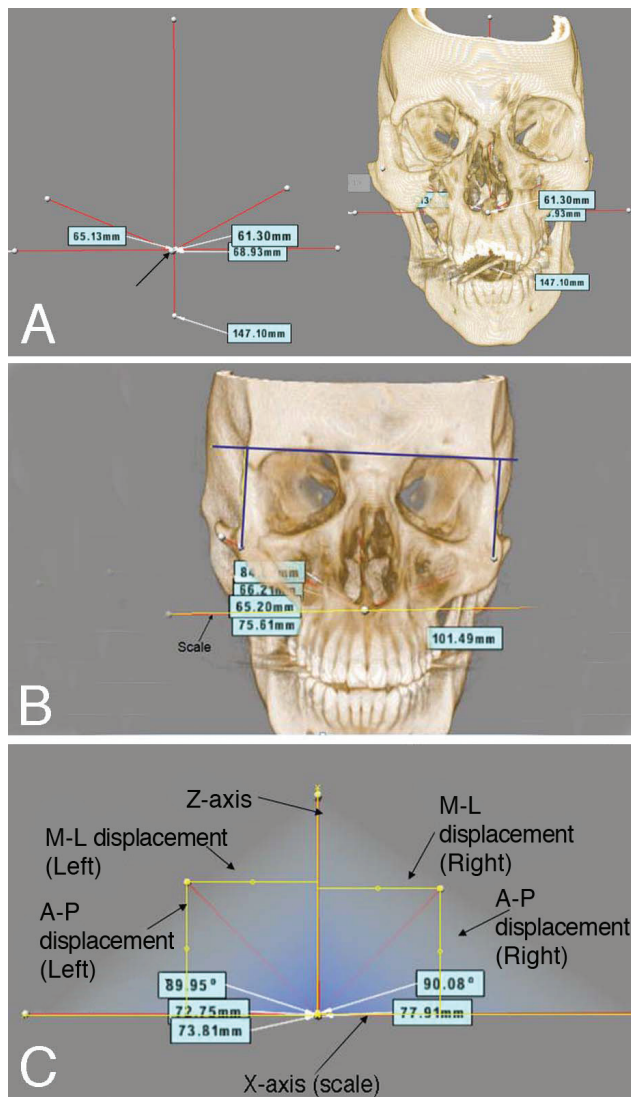


**Figure 33-2.** (A) Right orbital fracture identified as stemming from orbital-zygomatic-malar complex displacement; (B) orthogonal reference planes measured; and (C) displacement of fracture in all axes were measured. A-P: anterior-posterior; M-L: medial-lateral.

with errors caused by including the missing anterior wall of the orbit); (c) interoperator or intraoperator variability; and (d) errors caused by the use of different measurement techniques and software programs.

Recently, with the development of 3D software programs, it became easier to measure the orbital volume.

### ZYGOMATICOMAXILLARY COMPLEX FRACTURES

Due to the prominent midface location of the cheek, fractures of the zygomaticomaxillary complex (ZMC) represent the second most common type of facial fracture.<sup>12</sup> Traditionally referred to as a “tripod” fracture,

Ploder et al,<sup>7</sup> in their experimental studies using orbital fractured models on dried skulls, demonstrated that both 2-dimensional (2D) and 3D measurement methods are accurate for assessing the fracture area and herniated tissue volume of isolated blowout fractures, but they found that 2D-based calculations involved less processing time and fewer errors, thus improving surgical accuracy.

Few studies have examined the changes in orbital volume before and after surgery in patients with blowout fractures.<sup>6</sup> A 2009 study by Kwon et al<sup>12</sup> sought to evaluate orbital volume in such patients using two unique 3D analysis software packages (Vitreax Version 3.4, Vital Images Inc, Minnetonka, MN; and Dextroscope Version 1.0, Bracco AMT Inc, Princeton, NJ) to document the changes in orbital volume and to compare the accuracy of each system. The study group included 10 orbital floor fractures, 11 medial wall fractures, and 3 combined medial wall and floor fractures. All patients were treated with surgical repair. In cases involving orbital floor fractures, the fracture was exposed transantrally or transorbitally and supported by a porous polyethylene channel implant (Medpor Surgical Implant; Porex Surgical Products Group, Newnan, GA) or a bioresorbable perforated plate of 70:30 poly(L-lactide-co-D,L-lactide) (MacroPore; Medtronic Inc, Minneapolis, MN). For medial orbital wall fractures, endoscopic endonasal reduction surgery was performed using a Silastic (Dow Corning Corporation, Midland, MI) sheet splint or a MacroPore implant. CT examinations were performed on all patients before and after surgery, and charts were retrospectively reviewed. All images were obtained in a high-resolution osseous window level setting and transferred to the software programs. The software was used to configure area and volume. The mean (SD) normal orbital volumes calculated by Vitrea and Dextroscope were 25.5 (2.4) mL and 24.8 (3.0) mL, respectively. The average preoperative orbital volumes on the fractured side were 28.3 (2.3) mL and 27.6 (3.1) mL, respectively, while the postoperative volumes were 25.8 (2.5) mL and 24.9 (3.0) mL. The study found that consistent volume measurements can be obtained using different 3D image analysis programs. Measuring preoperative and postoperative volume changes and postoperative reduction can ensure a good surgical result and thereby decrease the incidence of enophthalmos.<sup>12</sup>

a ZMC fracture actually involves disruption at four sites: the lateral orbital rim, the inferior orbital rim, the zygomaticomaxillary buttress, and the zygomatic arch.<sup>3</sup> The majority of ZMC fractures are closed, dis-

placed, and noncomminuted.<sup>4</sup> Although the typical resultant deformity is a midface depression with posterior positioning of the malar prominence, a range of displacements, including anterior projection of the zygoma, may occur depending on the mechanism of trauma.<sup>5</sup> Because of the complex nature of ZMC fractures, which may be comminuted, involve multiple bones, or complicated by soft tissue edema, surgical repair is often challenging. In addition to malar asymmetry and other aesthetic sequelae, fractures of the ZMC may have substantial functional consequences, including concomitant orbital injury with ophthalmologic impairment, facial hypesthesia, and trismus, and are often associated with concomitant injuries to other parts of the craniofacial skeleton or spine.<sup>2,6,7</sup>

It has been suggested that all displaced ZMC fractures require surgical intervention, but conservative management is frequently employed in cases of minimal displacement, asymptomatic injury, likely patient noncompliance with follow-up, or medical contraindication to surgery.<sup>8,9</sup> No standard classification scheme currently exists to assist in assessing the severity of ZMC fractures or the need for surgical treatment. Although classification methods and treatment algorithms have been suggested, all are based on location of fracture lines rather than the degree and direction of displacement.<sup>5,10-12</sup> Similarly, radiographic evaluation of ZMC fractures is complicated by difficulties in translating a 3D rotation and displacement into a 2D imaging modality. In particular, the location of the malar eminence, which is critical to establishing facial symmetry, is challenging to pinpoint in 2D. The assessment of fracture severity from an aesthetic standpoint therefore remains a clinical judgment.

Pau et al<sup>13</sup> presented a novel method of ZMC fracture assessment, utilizing a 3D imaging modality to visualize and quantify malar eminence displacement in the anterior-posterior, medial-lateral, and superior-inferior dimensions. The pattern of malar displacement

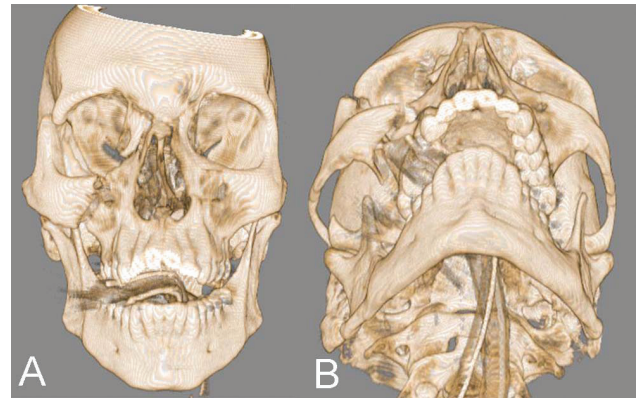


**Figure 33-3.** Right orbito-malar-zygomatic fracture shown as three-dimensional reconstruction in coronal and base view. The malar eminences are designated as the point of intersection between a vertical arc from the zygomatic process of the frontal bone to the maxilla superior to the first molar, and a horizontal arc from the inferior orbital rim along the superior aspect of the zygomatic arch.

was then correlated with the recommended surgical intervention. This allowed the authors to represent the clinical assessment of fracture severity, as well as the eventual outcome. The malar eminences were defined by the point of intersection between a vertical arc from the zygomatic process of the frontal bone to the maxilla superior to the first molar, and a horizontal arc from the inferior orbital rim along the superior aspect of the zygomatic arch (Figure 33-3). In fracture patients, the malar eminence on the fractured side was designated by inferring the location of the intersecting arcs on the displaced zygoma. Comparison of the left and right malar eminence positions in non-fracture subjects revealed a baseline anatomic variance in symmetry that can be compared in the medial lateral, superior-inferior, and anterior-posterior directions.<sup>13</sup> This study was a first step toward establishing a scientific, quantitative system for classifying ZMC fractures.

## MAXILLARY-MANDIBULAR RECONSTRUCTION

The greatest advancement seen in surgical planning involves the use of stereolithography models (SLMs). These models are based on 3D reformatting of CT images. They are used to analyze the patient by performing 3D measurements and to manipulate deformed or missing anatomy by mirror imaging, segmentation, or insertion of ideal skeletal constructs.<sup>14</sup> Stereolithography has been used in planning for reconstruction of facial defects caused by cancer to estimate the configuration, size, and positioning of free fibular osteocutaneous flaps. The models have also been used to plan for reconstruction of posttraumatic defects,

allowing the surgeon to contour the free tissue. This is particularly important when dental implantation is planned after surgery.

Leiggener et al<sup>15</sup> and Hirsch et al<sup>16</sup> recently described a protocol involving CAD/CAM software used to virtually plan mandibular reconstructions with fibular osteocutaneous free flaps and then transfer the idealized reconstruction to the patient using a selective laser sintering cutting guide. The modeling was performed on a computer in the preoperative setting, using Surgicase CMF software (Materialise, Leuven, Belgium), which enables the clinician to import 2D CT data in

DICOM format to a computer workstation and generate an accurate 3D representation of the skeletal and soft tissue anatomy. The dataset can be manipulated by segmentation, reflection, or insertion of specific anatomic regions for purposes of treatment planning, and then may be printed into an SLM. Transfer of the virtual plan to reality (implementation of the plan on a patient) is accomplished by utilizing custom surgical guide stents. CAD/CAM technology is used to print custom guide stents to optimize osteotomy placement

and position of the composite tissue construct or bone graft. The virtual data can also be imported into a navigation system (frameless stereotaxy), via a technique called “back-conversion,” which is used to further confirm the accurate and safe placement of hardware or bone grafts, movement of bone segments, resection of tumor, or osteotomy design. This intraoperative imaging also allows immediate dental implant placement, which theoretically increases the chance for successful prosthetic restoration and decreases treatment time.<sup>14</sup>

## SUMMARY

Modern preoperative planning has experienced a rapid transition from 2D CT-based analysis of orbital, orbito-zygomatic-malar, midface, and maxillary-mandibular trauma to 3D preoperative planning with intraoperative navigation in craniomaxillofacial reconstruction. Several manufacturers and software protocols provide options to help guide surgical re-

construction. The advantages of accurate diagnosis, establishing treatment plans, and correctly executing reduction and internal fixation of craniofacial deformities have driven protocols to transfer VSP to the operating room. The benefits of reduced operative time and accurate restoration for surgical patients make this new technology attractive.

## CASE PRESENTATIONS

### Case Study 33-1

#### Presentation

A 31-year-old healthy American contractor was traveling in Iraq when his vehicle was struck by an improvised explosive device (IED). The patient sustained a right mandibular body comminuted fracture. There was minimal mucosal loss in the region corresponding to the fracture site, and no significant overlying soft tissue loss.

#### Initial Operations and Complications

The patient was stabilized and returned stateside for definitive treatment. He initially underwent debridement of the area and open reduction internal fixation (ORIF) with a 2.0 locking titanium plate. He had traumatic loss of approximately 5 cm of mandibular bone involving the right body. Over the course of 15 months, he underwent nine separate surgical procedures involving various free, nonvascularized bone grafts to reconstruct this region. Unfortunately, the surrounding blood supply was severely compromised due to the high-energy blast of the IED, and all grafts underwent 100% absorption (Figure 33-4). Without viable bone spanning the region of the right mandibular body, the soft tissue envelope contracted, which resulted in superior displacement of the remaining ascending ramus, non-union, and severe pain with mastication (Figure 33-5). Dentate patients are able to generate

significant force upon mastication. In the absence of vascularized tissue, titanium hardware will inevitably fail over a course of 12 to 24 months. In this case, the locking screws extruded from the symphyseal region of the mandible (Figure 33-6).

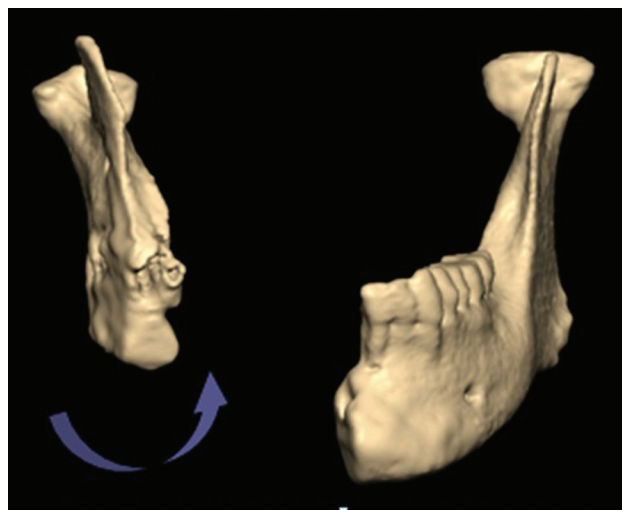


**Figure 33-4.** Three-dimensional image demonstrating absent 5-cm segment of the right mandibular body following an improvised explosive device blast. Previous nonvascularized bone grafts had reabsorbed due to inadequate blood supply. The subsequent loss of the soft tissue envelope resulted in rotation of the right ascending ramus (arrow).



**Figure 33-5.** Three-dimensional image demonstrating misaligned right ascending ramus. This rotational pull from scar contracture results when the soft tissue envelope is not maintained. The *gray mandibular shadow* is the mirror image of the uninjured contralateral left mandible and serves to demonstrate the premorbid position of the condylar head and mandibular angle.

### Virtual Planning and Reconstruction

Approximately 16 months following the initial injury, the patient was referred to the head and neck

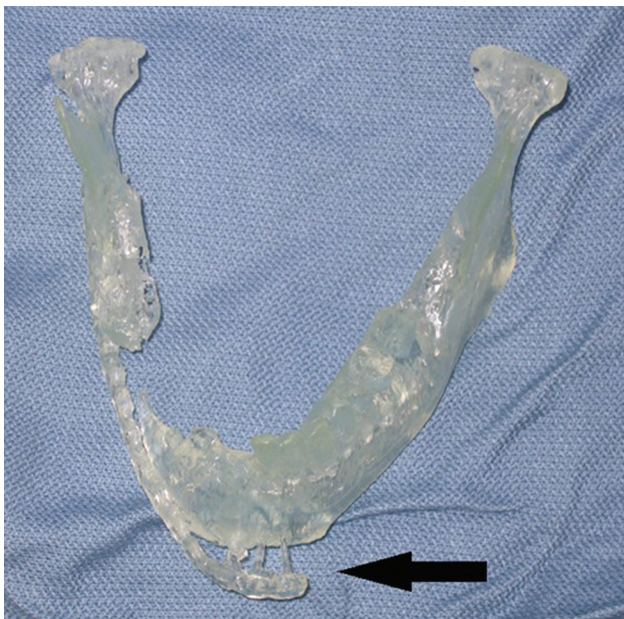


**Figure 33-6.** Three-dimensional stereolithic model demonstrating right mandibular body defect following loss of nonvascularized bone grafts. Screws are extruding from the locking titanium plate (*arrow*) due to the lack of vascularized tissue in the setting of masticatory forces.

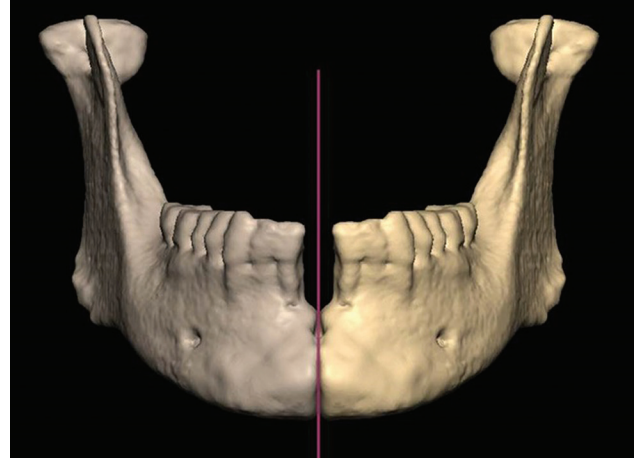


**Figure 33-7.** Computer-generated reconstruction of the presumed premorbid mandible using mirror imaging of the noninjured left hemimandible (compare to Figure 33-1).

reconstructive surgeon at Wilford Hall Medical Center, San Antonio, for the evaluation of free-tissue transfer. His initial preoperative workup entailed a noncontrast fine-cut CT scan of the face, with 3D reformatting (see similar cases in Figures 33-1 and 33-2). The prosthodontics team utilized this imaging to construct a 3D SLM (see Figure 33-6).

In an effort to restore native occlusion, computer software was used to manipulate CT imaging data to recreate the presumed premorbid mandible from a mirror image of noninjured left side (Figure 33-7). This image was then used to create a new 3D SLM that closely approximated the preinjury craniofacial skeleton (Figure 33-8). Because the native bone had been missing for over 15 months and the corresponding soft tissues were scarred, this 3D SLM was used to pre-bend the template and ultimately the 2.4 titanium locking mandibular reconstruction plate in preparation for intraoperative ORIF.

The patient was brought to the operating room for wound debridement, scar excision, and removal of failed hardware. Debridement continued until healthy bleeding bone was observed in the region of both the posterior mandibular body and the symphyseal region (Figure 33-9). Because all previous nonvascularized bone grafts had failed, the patient underwent mandibular reconstruction using a fibular free flap. Prior to flap harvest, magnetic resonance angiography was used to confirm adequate three-vessel run-off to the foot. ORIF was achieved using the pre-bend 2.4 titanium locking mandibular reconstruction plate, which also facilitated the fibula free flap inset.

The surgery and postoperative course were uncom-



**Figure 33-8.** Three-dimensional stereolithographic model generated using the mirror image of the noninjured left hemimandible. This model was used to bend the template (purple) and ultimately the 2.4 titanium locking mandibular reconstruction plate (gold).

plicated. Three months following surgery, the patient underwent successful dental rehabilitation using osseocutaneous implants within the fibula bone graft to secure his denture (Figure 33-10). He had normal occlusion following this reconstruction, resumed all of his nutrition orally, and was eating pain free.

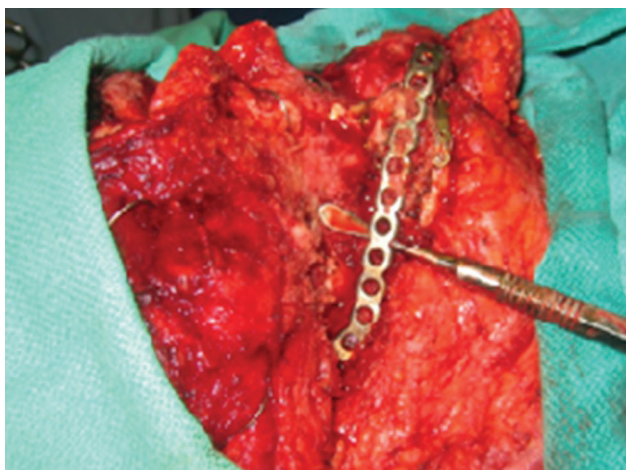


**Figure 33-9.** Intraoperative findings of right mandibular non-union secondary to free bone graft reabsorption. The old hardware present in this picture was removed and replaced by a 2.4 titanium locking plate (depicted in Figure 33-8).

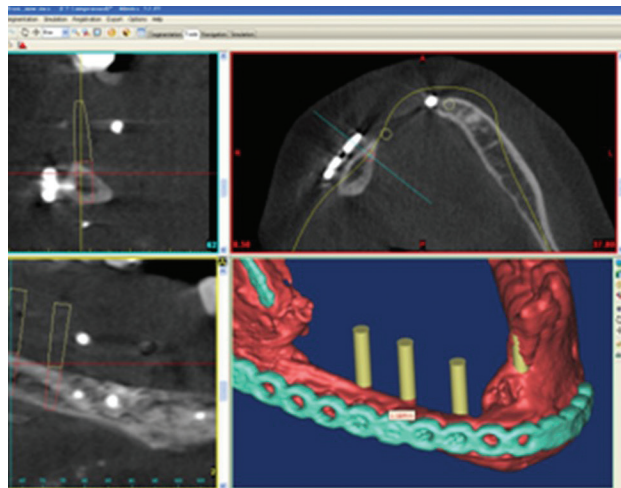


**Figure 33-10.** Computer planning for dental rehabilitation. Note that despite the difference in bony height between the native mandible and fibula, osseointegrated implants can be placed in the graft (gold cylinders).

### Lessons Learned

This case serves to demonstrate the important role of CT imaging and SLM in the reconstruction of craniomaxillofacial trauma. This advanced technology becomes extremely important in delayed reconstruction, when bone has been missing for an extensive period of time, thus causing loss of the soft tissue envelope and subsequent scar contracture. Models developed using fine-cut mirror images of the uninjured side allow for restoration of normal occlusion; this technique is far more precise than a reconstruction plate hand bent in the operating room using surgeon estimations.

This case also demonstrates the advanced technology implemented in dental rehabilitation. Using CT data and computer software, osseointegrated implantation can be optimized to avoid free flap osteotomy sites and screws. This diligent preoperative planning optimizes the success of dental restoration, which can be challenging in the setting of war injuries.

### Case Study 33-2

#### Presentation

An otherwise healthy 40-year-old active duty soldier serving in Operation Enduring Freedom sustained an IED blast injury to the face while traveling in his Humvee. He sustained significant soft tissue injuries including burns to his face, loss of his right oral commissure and surrounding upper and lower lips, avulsion of his nasal tip, loss of his right buc-

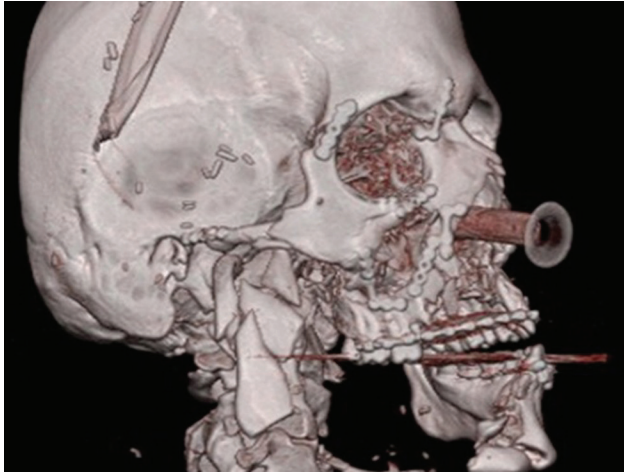


**Figure 33-11.** Three-dimensional computed tomography reformatting of the craniomaxillofacial region following improvised explosive device (IED) blast. Initial debridement and the first stage of reconstruction were completed prior to this imaging. Injuries included comminuted fractures of the right mandible, zygomaticomaxillary complex, and orbital walls. This fracture pattern is common in high-energy IED blasts.

cal mucosa, and loss of his right floor of mouth. The high-energy blast injury resulted in significant fractures to the right craniomaxillofacial region (Figure 33-11). His right mandible from the condyle to the right parasymphaseal region was severely fractured, and a nonviable portion of bone was removed during the initial debridement. He also sustained traumatic loss of his right maxillary alveolar ridge, comminuted fracture of the right ZMC, a right Le Fort III fracture, and right orbital wall fractures.

In addition to the above facial trauma, the patient also sustained multiple orthopedic injuries to his hands and a severe traumatic brain injury, necessitating intense specialized inpatient rehabilitation. The patient's definitive facial reconstruction was delayed, and tissue contracture developed. The loss of bone in the region of the right mandibular body resulted in collapse of the soft tissue envelope in this region, limited jaw range of motion, a significant cross bite, and difficulties with mastication.

### *Virtual Planning and Reconstruction*

After completing traumatic brain injury rehabilitation, the first stage of the reconstruction focused on restoring the native mandibular contour. Planning incorporated 3D CT imaging to recreate the missing mandibular bone using a mirror image of the uninjured left side. A custom SLM was then fashioned using the mirrored imaging (Figure 33-12). A 2.4 locking titanium mandibular reconstruction plate was bent



**Figure 33-12.** Stereolithographic model built using computed tomography mirror imaging to recreate the missing right hemimandible. From this model, a 2.4 titanium locking mandibular reconstruction plate was pre-bent in preparation for free flap reconstruction.

to fit the SLM. In doing so, a precise recreation of the mandibular arch was achieved.

Using fine-cut CT imaging, it was estimated that the patient had lost approximately 8 cm of bone in the region of his right mandibular angle and body. Given the amount of missing bone, devascularized surrounding tissue resulting from the IED blast, and desire to achieve dental restoration, the decision was made to reconstruct the area using a fibular free-tissue transfer. Prior to harvesting the flap, three-vessel run-off to the lower extremities was confirmed using magnetic resonance angiography.

The patient was brought to the operating room and administered general anesthesia using a previously placed tracheostomy tube. He underwent aggressive debridement of his scar and all remaining devascularized mandibular bone. His severe cross bite resolved after scar resection, and his remaining dentition was held in native occlusion using intermaxillary fixation screws (Figure 33-13). ORIF of the mandibular fracture was achieved using bicortical locking screws and the pre-bent titanium plate.

The osseocutaneous fibular free flap (Figure 33-14) was harvested in the standard fashion. One osteotomy was required to recreate the right parasymphaseal region. A portion of the fibula skin paddle was used to recreate the intraoral lining, while the remaining cutaneous portion was used for external coverage.

Dental restoration began 3 months following the fibula free-tissue transfer. This reconstruction required a team approach including the head and neck surgeon,

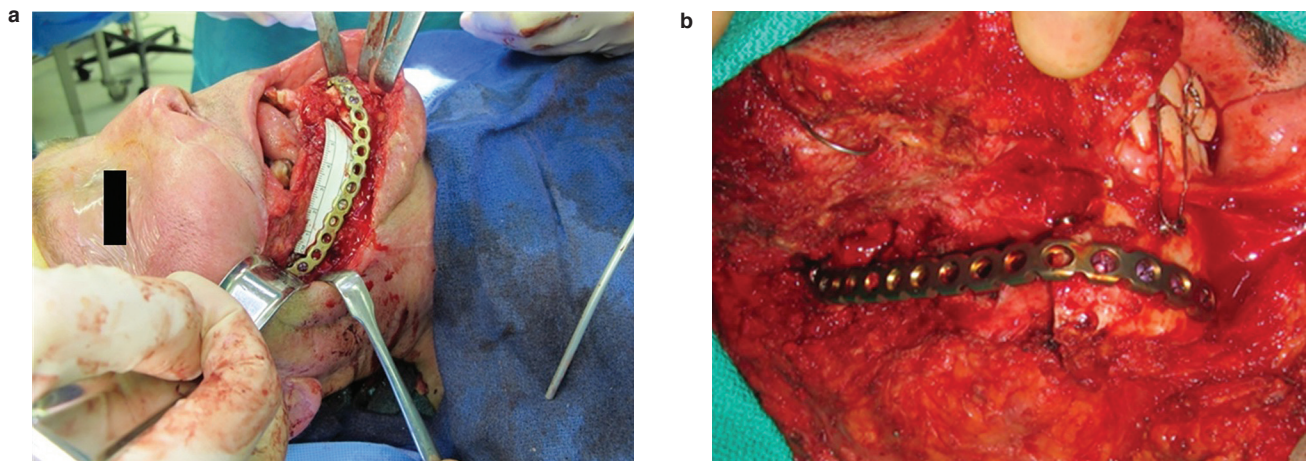


**Figure 33-13.** (a) Intraoperative photo demonstrating 8 cm of missing mandibular bone involving the right angle and body. (b) Following scar resection, native occlusion was achieved and held using intermaxillary fixation screws. The pre-bent 2.4 locking titanium reconstruction bar was secured using bicortical screws in the native mandible.

plastic surgeon, oral surgeon, prosthodontist, and speech therapist. Three osseointegrated posts were placed in the fibula graft to retain a lower denture



**Figure 33-14.** Osseocutaneous fibula free flap harvested for mandibular reconstruction. The skin paddle was used for both internal and external coverage.

(Figure 33-15). Radiographic and intraoperative assessment demonstrated significant maxillary bone stock for osseointegrated implantation. Stereolithographic modeling performed by the prosthodontics team was used to create intraoperative guides for maxillary implant placement. Following the staged osseointegrated implants, the patient was able to wear both a maxillary and mandibular denture (Figure 33-16). He achieved oral competency, was able to maintain all nutrition orally, had his percutaneous endoscopic gastrostomy tube removed, and was decannulated. He was pleased with his cosmetic appearance and returned home.

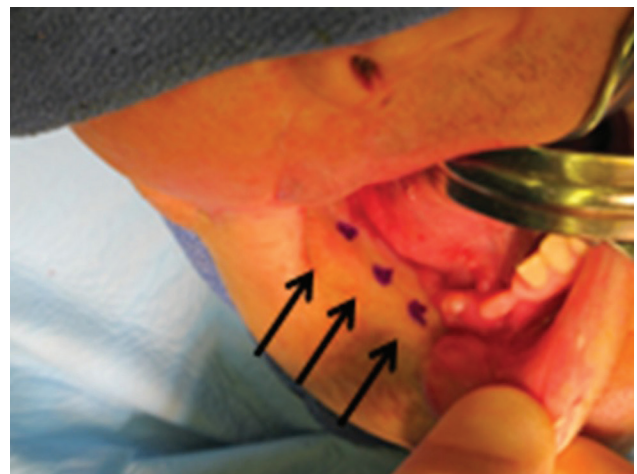


**Figure 33-15.** Three months following right mandibular reconstruction with an osseocutaneous fibula free flap. The skin paddle was used to recreate the intraoral lining. Arrows denote location of future osseointegrated implants for dental restoration.



**Figure 33-16.** Six months following fibula free flap. The patient successfully underwent maxillary and mandibular dental restoration with osseointegrated implants to retain dentures. He achieved oral competency and resumed all nutrition orally.

### Lessons Learned

This case highlights the important role of CT imaging and SLMs in the reconstruction of combined mandibular and maxillary trauma. The mirror images and associated models of missing bone allow for precise restoration of the mandibular arch and, therefore, native occlusion. It is important to remember that if occlusion is off by even a millimeter, the patient with dentition will be aware of the malposition. In addition, SLMs allow for titanium plates to be pre-bent, thereby saving time in the operating room.

This case also highlights the team approach required in preoperative planning. A close working relationship among otolaryngology, oral surgery, plastic surgery, dentistry, prosthodontics, and speech is imperative to optimize outcomes. Lastly, it is extremely important for the patient and his or her family to understand that definitive reconstruction requires extensive preoperative planning and multiple surgeries that will likely span an entire year.

### Acknowledgments

The authors would like to thank the lead maxillofacial prosthodontist, Dr Alan Sutton, for his expert reconstruction in the cases presented.

### REFERENCES

1. Levine JP, Patel A, Saadeh PB, Hirsch DL. Computer-aided design and manufacturing in craniomaxillofacial surgery: the new state of the art. *J Craniofac Surg.* 2012;23(1):288–293.
2. Raskin EM, Millman AL, Lubkin V, della Rocca RC, Lisman RD, Maher EA. Prediction of late enophthalmos by volumetric analysis of orbital fractures. *Ophthal Plast Reconstr Surg.* 1998;14:19–26.
3. Charteris DG, Chan CH, Whitehouse RW, Noble JL. Orbital volume measurement in the management of pure blowout fractures of the orbital floor. *Br J Ophthalmol.* 1993;77:100–102.
4. Deveci M, Ozturk S, Sengezer M, Pabuscu Y. Measurement of orbital volume by a 3-dimensional software program: an experimental study. *J Oral Maxillofac Surg.* 2000;58:645–648.
5. Fan X, Li J, Zhu J, Zhang D. Computer-assisted orbital volume measurement in the surgical correction of late enophthalmos caused by blowout fractures. *Ophthal Plast Reconstr Surg.* 2003;19:207–211.
6. Whitehouse RW, Batterbury M, Jackson A, Noble JL. Prediction of enophthalmos by computed tomography after ‘blow out’ orbital fracture. *Br J Ophthalmol.* 1994;78:618–620.
7. Ploder O, Klug C, Voracek M, Burggasser G, Czerny C. Evaluation of computer-based area and volume measurement from coronal computed tomography scans in isolated blowout fractures of the orbital floor. *J Oral Maxillofac Surg.* 2002;60:1267–1272; discussion 1273–1274.
8. Furuta M. Measurement of orbital volume by computed tomography: especially on the growth of the orbit. *Jpn J Ophthalmol.* 2001;45:600–606.

9. Ahn HB, Ryu WY, Yoo KW, et al. Prediction of enophthalmos by computer-based volume measurement of orbital fractures in a Korean population. *Ophthal Plast Reconstr Surg*. 2008;24:36–39.
10. Calhoun PS, Kuszyk BS, Heath DG, Carley JC, Fishman EK. Three-dimensional volume rendering of spiral CT data: theory and method. *Radiographics*. 1999;19:745–764.
11. Kwon J, Barrera JE, Most SP. Comparative computation of orbital volume from axial and coronal CT using three-dimensional image analysis. *Ophthal Plast Reconstr Surg*. 2010;26:26–29.
12. Kwon J, Barrera JE, Jung TY, Most SP. Measurements of orbital volume change using computed tomography in isolated orbital blowout fractures. *Arch Facial Plast Surg*. 2009;11(6):395–398. doi:10.1001/archfacial.2009.77.
13. Pau, C, Barrera JE, Kwon J, Most SP. Three-dimensional analysis of zygomatic-maxillary complex fracture patterns. *Craniofacial Trauma Reconstr*. 2010;3(3):167–176. doi:10.1055/s-0030-1263082.
14. Markiewicz MR, Bell RB. modern concepts in computer-assisted craniomaxillofacial reconstruction. *Curr Opin Otolaryngol Head Neck Surg*. 2011;19:295–301.
15. Leiggenger C, Messo E, Thor A, Zeilhofer HF, Hirsch JM. A selective laser sintering guide for transferring a virtual plan to real time surgery in composite mandibular reconstruction with free fibula osseous flaps. *Int J Oral Maxillofac Surg*. 2009;38:187–192.
16. Hirsch DL, Garfein ES, Christensen AM, Weimer KA, Saddeh PB, Levine JP. Use of computer-aided design and computer-aided manufacturing to produce orthognathically ideal surgical outcomes: a paradigm shift in head and neck reconstruction. *J Oral Maxillofac Surg*. 2009;67:2115–2122.